AGU PUBLICATIONS

Geophysical Research Letters

RESEARCH LETTER
10.1002/2015GL064665

Key Points:
- LdM has been experiencing a spectacular unrest episode for more than 8 years
- More than 1.8 m of vertical displacement has accumulated since 2007
- LdM resembles other volcanic systems in temporal evolution of deformation

Supporting Information:
- Figure S1
- Figure S2
- Figure S3
- Figure S4
- Figure S5
- Figure S6
- Figure S7
- Figure S8
- Figure S9
- Texts S1 and S2, Figures S1–S9, and Tables S1–S3

Correspondence to:
H. Le Mével,
lemevel@wisc.edu

Citation:
Le Mével, H., K. L. Feigl, L. Córdova, C. DeMets, and P. Lundgren (2015), Evolution of unrest at Laguna del Maule volcanic field (Chile) from InSAR and GPS measurements, 2003 to 2014, *Geophys. Res. Lett.*, *42*, doi:10.1002/2015GL064665.

Received 26 MAY 2015
Accepted 8 JUL 2015
Accepted article online 14 JUL 2015

©2015. The Authors.
This is an open access article under the terms of the Creative Commons Attribution-NonCommercial-NoDerivs License, which permits use and distribution in any medium, provided the original work is properly cited, the use is non-commercial and no modifications or adaptations are made.

Evolution of unrest at Laguna del Maule volcanic field (Chile) from InSAR and GPS measurements, 2003 to 2014

Hélène Le Mével[1], Kurt L. Feigl[1], Loreto Córdova[2], Charles DeMets[1], and Paul Lundgren[3]

[1]Department of Geoscience, University of Wisconsin-Madison, Madison, Wisconsin, USA, [2]Observatorio Volcanológico de los Andes del Sur, SERNAGEOMIN, Temuco, Chile, [3]Jet Propulsion Laboratory, California Institute of Technology, Pasadena, California, USA

Abstract The Laguna del Maule (LdM) volcanic field in the southern volcanic zone of the Chilean Andes exhibits a large volume of rhyolitic material erupted during postglacial times (20–2 ka). Since 2007, LdM has experienced an unrest episode characterized by high rates of deformation. Analysis of new GPS and Interferometric Synthetic Aperture Radar (InSAR) data reveals uplift rates greater than 190 mm/yr between January 2013 and November 2014. The geodetic data are modeled as an inflating sill at depth. The results are used to calculate the temporal evolution of the vertical displacement. The best time function for modeling the InSAR data set is a double exponential model with rates increasing from 2007 through 2010 and decreasing slowly since 2010. We hypothesize that magma intruding into an existing silicic magma reservoir is driving the surface deformation. Modeling historical uplift at Yellowstone, Long Valley, and Three Sisters volcanic fields suggests a common temporal evolution of vertical displacement rates.

1. Introduction

Inflationary processes occur at numerous volcanoes in a broad range of tectonic settings prior to eruptive events (e.g., Okmok [*Lu et al.*, 2000] and Kīlauea [*Cayol et al.*, 2000]) or intrusive episodes (e.g., dike injections during the rifting episodes at Krafla and Dabbahu [e.g., *Grandin et al.*, 2009; *Wright et al.*, 2012]). Deformation of the volcanic edifice is usually interpreted in terms of magma dynamics (mass flux and/or pressurization) that may presage an eruption [e.g., *Sparks*, 2003; *Dzurisin*, 2007]. In other cases, however, repeated cycles of measurable ground motion are observed without any subsequent magmatic events. For example, the caldera-scale silicic volcanic system of Campi Flegrei, Italy, inflated by more than 1.5 m between 1982 and 1984 but did not erupt [e.g., *Trasatti et al.*, 2011; *Del Gaudio et al.*, 2010]. Recently, satellite geodetic measurements from Interferometric Synthetic Aperture Radar (InSAR) and the Global Positioning System (GPS) have shown significant crustal deformation above other large silicic volcanic systems such as Yellowstone (USA) [*Chang et al.*, 2007, 2010], Santorini (Greece) [e.g., *Newman et al.*, 2012; *Parks et al.*, 2012; *Papoutsis et al.*, 2013], and Uturuncu (Bolivia) [e.g., *Henderson and Pritchard*, 2013; *Pritchard and Simons*, 2002; *Walter and Motagh*, 2014].

In the Southern Volcanic Zone of the Chilean Andes between 34° and 36°S, several large-volume silicic eruptions have occurred during the Quaternary behind the volcanic front. These include the Maipo-Diamante caldera, the Calabozos caldera, the Puelche volcanic field, and the Laguna del Maule (LdM) volcanic field [*Hildreth et al.*, 1999, 2010]. The LdM volcanic field covers 500 km^2 and includes 350 km^3 of material erupted in the last 1.5 Ma, ranging from basalt to rhyolite and including caldera collapses at 1.5 Ma and 950 ka [*Hildreth et al.*, 2010]. Postglacial volcanism over the last 20 ka has been characterized by a concentration of modest (<1.3 km^3) effusive and explosive rhyolitic eruptions and a dearth of mafic-to-intermediate lavas [*Hildreth et al.*, 2010]. The result is an exceptional spatial and temporal concentration of rhyolite that is unique in the Andes [*Singer et al.*, 2014].

An inflationary event centered between several of the postglacial rhyolite vents of the LdM volcanic field began some time after 2004 but no later than 2007, based on InSAR measurements [*Fournier et al.*, 2010]. Subsequently, the rate of vertical uplift exceeded 250 mm/yr through January 2012 [*Feigl et al.*, 2014]. Here we use an extended data set with three additional years of GPS and InSAR measurements to update the time series of deformation from that published by *Feigl et al.* [2014], to introduce a double exponential model of the temporal evolution of uplift, and to compare the character of Laguna del Maule deformation to that of other restless systems.

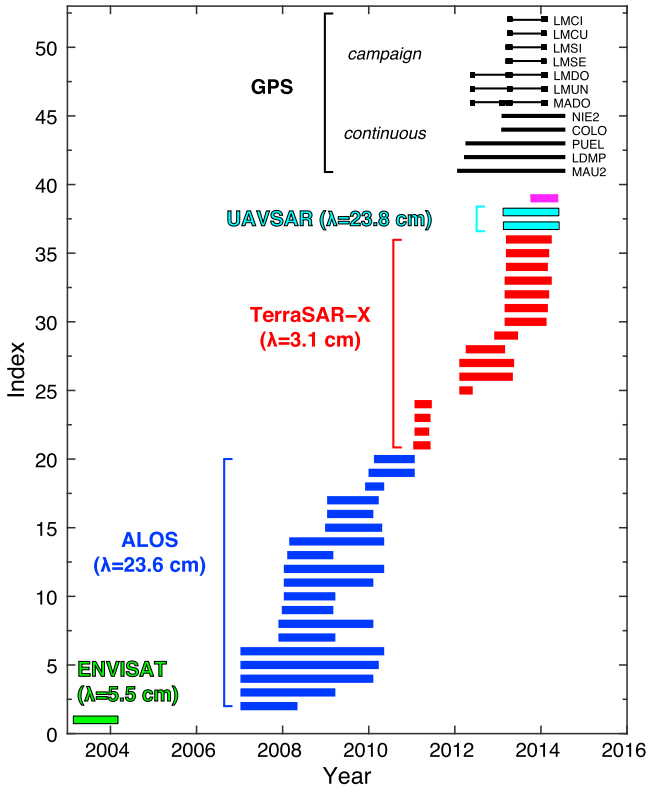

Figure 1. Geodetic data used in this study. InSAR pairs are shown as colored rectangles; each color indicates a different Synthetic Aperture Radar (SAR) mission. Time spanned by GPS measurements are shown as black lines; each square represents one occupation of a campaign site. COSMO-Skymed stack includes 71 interferograms. Details appear in Table S1 in the supporting information.

2. Methods

Our InSAR data set includes 37 interferometric pairs from four satellite missions (Figure 1 and Table S1 in the supporting information). Interferograms from the ENVISAT, ALOS, and TSX/TDX missions were calculated using the DIAPASON software developed at the French Space Agency CNES [*Massonnet*, 1997] (Text S1). COSMO-Skymed data were analyzed using the InSAR Scientific Computing Environment (ISCE) (Text S1 and Figure S1). In addition, the Uninhabited Aerial Vehicle Synthetic Aperture Radar (UAVSAR) system flew over LdM in 2013 and 2014, allowing the calculation of two interferograms (Table S1 and Figure S2). The UAVSAR data were processed by the UAVSAR project at the Jet Propulsion Laboratory (JPL) (Text S1). To estimate the model parameters that best fit each interferometric pair, we use the General Inversion of Phase Technique (GIPhT), as developed by *Feigl and Thurber* [2009] and extended by *Ali and Feigl* [2012] (e.g., Figure S3). To simulate the deformation, we use the same model of an expanding sill in a half-space with uniform elastic properties via a dislocation formulation [*Okada*, 1985], as described by *Feigl et al.* [2014]. The model includes eight parameters for the dislocation and three "nuisance" parameters to account for the phase gradient vector.

We then estimate the best fitting values of the 11 model parameters for each interferometric pair, following the same procedure as in *Feigl et al.* [2014]. Using these estimates, we calculate the modeled rate of vertical displacement for the time interval corresponding to each of the 39 interferometric pairs (Figure 2a). To evaluate their time dependence, we then perform a time series analysis using temporal adjustment, as in *Feigl et al.* [2014]. As described in previous studies, this procedure converts the rate of (relative) vertical displacement estimated over several time intervals into the total (absolute) displacement at each point ("epoch") in time [e.g., *Beauducel et al.*, 2000; *Schmidt and Bürgmann*, 2003; *Feigl and Thurber*, 2009; *Grandin et al.*, 2009]. The temporal adjustment is implemented in Matlab by the GraphTreeTA software (E. Baluyut et al. "Graph theory for analyzing pair-wise data: Application to interferometric synthetic aperture radar at Okmok volcano, Alaska," manuscript in preparation, 2015). In the case of LdM, we consider several parameterizations to model the cumulative uplift from 2007 through 2014, including: (a) a constant rate (Figure S4), (b) a piecewise linear

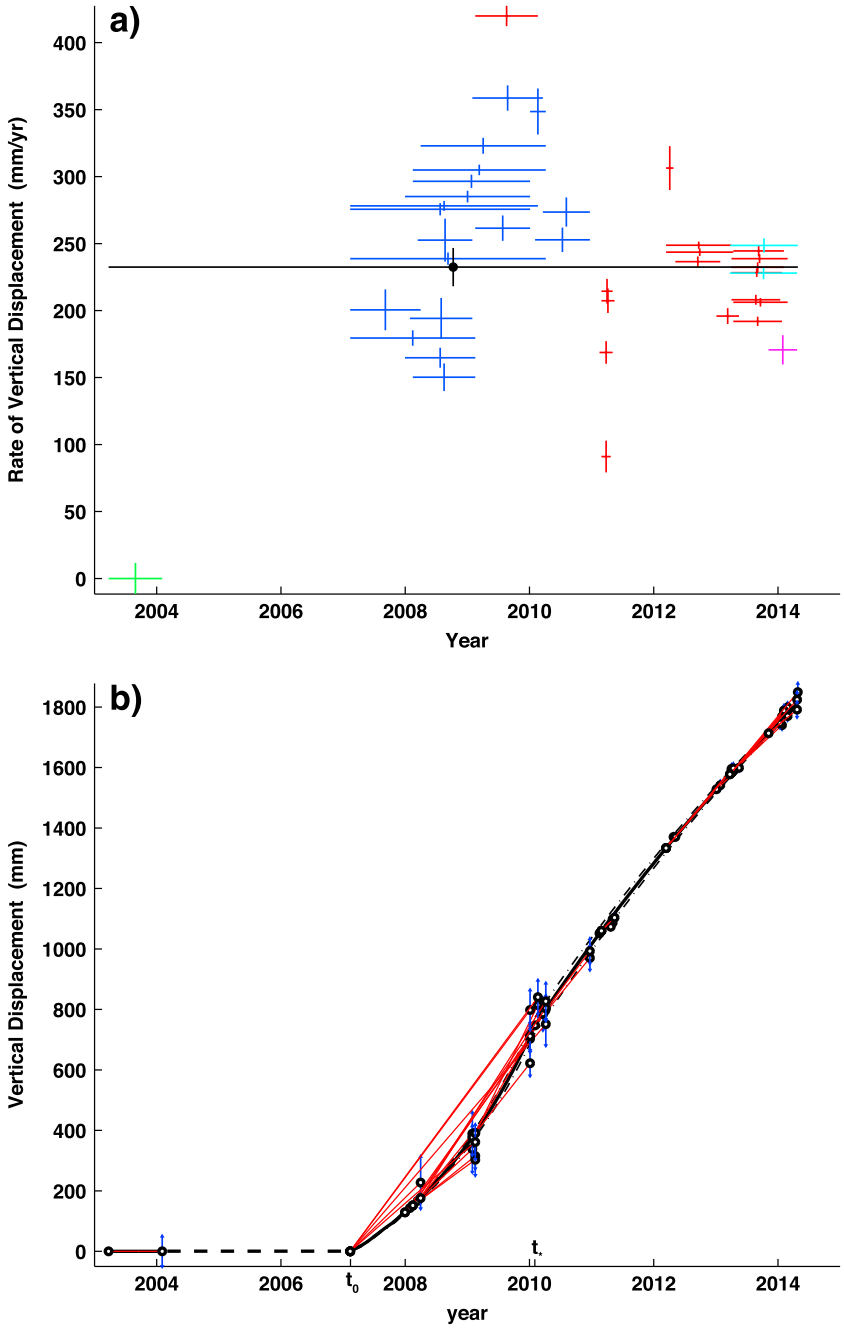

Figure 2. (a) Vertical displacement rates (colored bars) for each calculated InSAR pair from the best fitting estimates of the model parameters for that pair and their weighted mean (black circle). Colors indicate satellite mission as in Figure 1. (b) Time series (black curve) of cumulative vertical displacement for a point located at GPS station MAU2 from 2003 to 2014, as derived from InSAR data and assuming a double exponential model (equations (1) and (2)). Black dashed line is the 69% confidence interval for the modeled black curve. Each red segment represents an individual InSAR pair connecting two SAR epochs (black circles). In each InSAR pair, the value of displacement is plotted to fall on the model curve and the value of relative displacement at the second epoch is plotted with its 69% confidence interval (vertical blue bars).

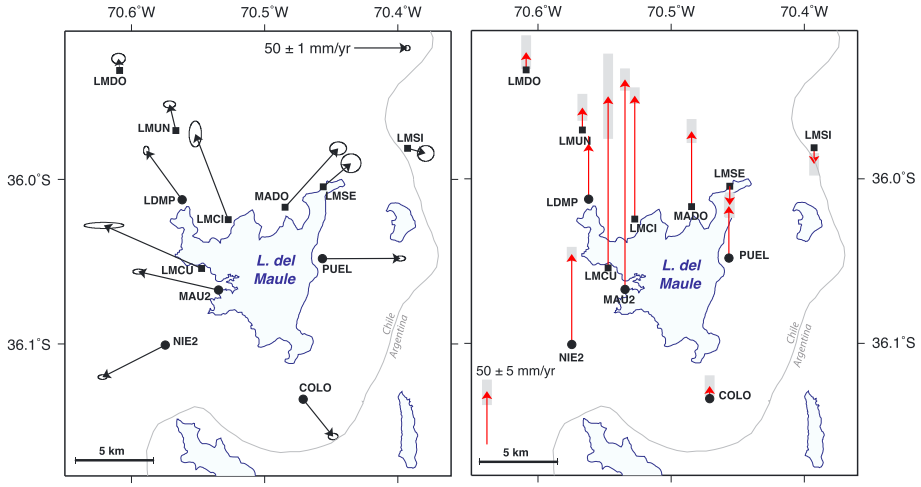

Figure 3. Velocity field estimated at permanent GPS (circles) and campaign (squares) sites with respect to the continuous GPS site MAUL, located 30 km NNW of Laguna del Maule, outside the actively deforming area. (left) Horizontal velocity field estimated from GPS data recorded between February 2013 and July 2014 (black arrows). Ellipses denote 95% confidence. (right) Vertical component of the velocity field over the same time interval (red arrows). Thick gray bars indicate the 95% confidence interval for each vertical rate.

adjustment (Figure S5), and (c) a double exponential parameterization consisting of an exponentially increasing rate followed by an exponentially decreasing rate via equations (1) and (2) (Figure 2b).

GPS measurements at Laguna del Maule, including data from five continuous sites installed by Observatorio Volcanológico de los Andes del Sur (OVDAS) in 2012 and 2013 (Figure 3), allow us to track deformation even during the ~7 months per year when the snow cover on the ground causes SAR images to decorrelate. The GPS data were analyzed with the GIPSY software (release 6.2) from JPL (Text S2, Figure S6, Tables S2, and S3).

3. Evolution of the Unrest Episode

Eight years of InSAR acquisitions and 2.5 years of continuous GPS measurements constrain the spatial distribution and temporal evolution of the deformation. For interpretation, we divide the time series into several intervals separated by changes in deformation rates.

3.1. The Onset

When did the current episode of rapid deformation begin? To answer this question, we consider interferometric combinations of SAR data acquired between 2004 and 2007 by several satellites. For images acquired before 2003 or between 2004 and 2007, no coherent interferogram could be made. A single ENVISAT interferogram spanning 2003 to 2004 indicates that the deformation had not yet begun in March 2004, as first noticed by *Fournier et al.* [2010]. In the following time series analysis, we assume that the deformation began in February 2007 (t_0 on Figures 2, S4, and S5), at the first SAR epoch of the InSAR pair showing deformation. Thus, the estimated value of the total accumulated displacement is a lower bound. The InSAR time series was calculated for the pixel corresponding to the location of the continuous station MAU2 (Figures 2 and 3).

3.2. From 2007 to Early 2010: Exponentially Increasing Rates

The rate of uplift increased rapidly through March 2010. Of the three parameterizations that we tested for this period, the following expression best fits the displacements inferred from the InSAR data:

$$u(t) = a_1 \exp[(t - t_0)/\tau_1] \qquad \text{for } t_0 \le t < t_*, \tag{1}$$

where the magnitude $a_1 = 304$ mm and the characteristic time constant $\tau_1 = 2.4$ years. The fit is significantly better with 95% confidence than using a constant rate of 240 ± 6 mm/yr for the same time interval (Figure S4), as calculated by an *F* test [*Wackerly et al.*, 2007]. This time interval is thus characterized by an accelerating rate of uplift.

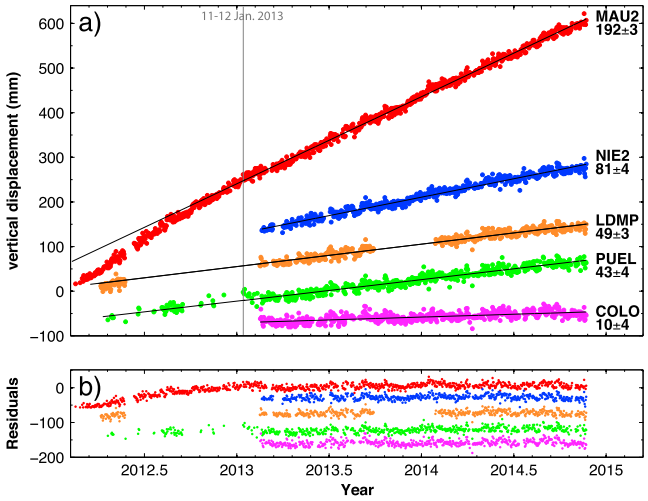

Figure 4. Vertical displacement time series for five continuous GPS stations, showing (a) observed position and (b) residual position calculated by subtracting the best fitting linear trend from January 2013 to November 2014, with respect to station MAUL. Daily vertical position uncertainties are smaller than the symbols. Gray line indicates the seismic swarm of 11–12 January 2013. Labels indicate displacement rate in mm/yr.

3.3. From 2010 to Late 2014: Exponentially Decaying Rates

3.3.1. InSAR

Between March 2010 and February 2011, the vertical displacement rate decreased to approximately 220 mm/yr. We estimate the time t_* of this transition to occur in March 2010 (Figure 2). Subsequently, the displacement is modeled as:

$$u(t) = a_2 \exp[-(t - t_*)/\tau_2] \qquad \text{for } t \geq t_*, \tag{2}$$

where $a_2 = -3058$ mm and $\tau_2 = 10$ years. During this 4 year interval, the characteristic time constant τ_2 is much longer than τ_1, consistent with a nearly linear temporal evolution of the vertical displacement after 2010.

3.3.2. GPS (March 2012 to November 2014)

Beginning in March 2012, the GPS stations show high rates of uplift and horizontal displacement radiating outward from the SW region of the lake (Figures 3 and 4). The velocities of stations MAU2 and PUEL changed in January 2013, as shown by the different slopes prior to 2013 (Figure 4b). These changes in velocity are significantly different from zero with 95% confidence, as indicated by a two-tailed *t* test [*Wackerly et al.*, 2007]. The vertical velocities at MAU2 and PUEL are 26% and 22% higher before 2013, respectively. The deceleration coincided with a swarm of more than 200 volcano-tectonic (VT) seismic events on 11–12 January 2013, the largest yet recorded at LdM by OVDAS [*Singer et al.*, 2014].

Figures 3 and 4 show the motion of the GPS stations estimated from January 2013 to October 2014. Station MAU2 moves upward at 192 ± 3 mm/yr with respect to MAUL in the far field, more rapidly than any other site. The horizontal velocity is highest at campaign site LMCU with 100 ±7 mm/yr toward the NW. The small (<10 mm) zero-centered residuals (Figure 4b) confirm that the vertical displacement has been linear in time since early 2013. The residual motions of all five continuous GPS stations include similar oscillations, indicating a local source of seasonal effects that could be associated with changes in lake level, temperature, snow cover, or a combination of the three.

4. Discussion

The spatial pattern revealed by the GPS and InSAR data (Figure 3) is consistent with radial expansion of a source at depth below the central southwest region of the lake, between the andesitic peninsula, and the youngest rhyolite flow to the south (units *apj* and *rln*, as mapped by *Hildreth et al.* [2010] and shown by *Singer et al.* [2014]). The ratio of maximum horizontal to vertical displacement is ~35%, indicating an elongated source, as sill geometries tend to create more vertical displacement [e.g., *Dieterich and Decker*, 1975; *Davis*, 1986]. The horizontal gradient of velocity (strain rate) is $\sim 3 \times 10^{-6}$/yr and 20×10^{-6}/yr for the horizontal and vertical components of velocity, respectively. The spatial extent of the inflation pattern as revealed by InSAR is about

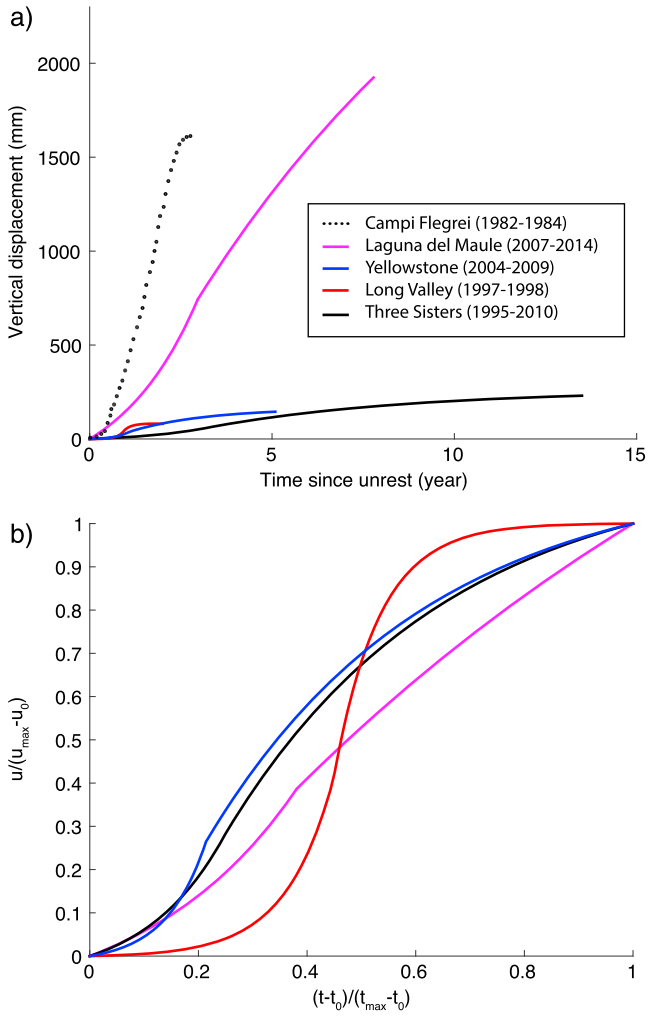

Figure 5. (a) Best models of vertical displacement time series from GPS or InSAR for the three other studied uplift episodes: Yellowstone caldera, WY (USA) (original GPS data from USGS, Figure S4), Three Sisters volcanic center, OR (USA) (data from *Riddick and Schmidt* [2011] and Figure S5), and Long Valley caldera, CA (USA) model from *Newman et al.* [2001]. Vertical ground movement data from Campi Flegrei (Italy) [*Berrino et al.*, 1984; *Bianchi et al.*, 1987; *Orsi et al.*, 1999] are represented for comparison but not modeled; (b) normalized uplift u' (equation (3)) as a function of normalized time t' (equation (4)) since the beginning of unrest.

20 by 26 km, affecting the entirety of the postglacial portion of the volcanic field. These observations suggest that processes within a large magma reservoir underlying the LdM volcanic field are driving the deformation. Geological observations, such as the spatial and temporal distribution of the recent silicic eruptive vents, also support the hypothesis of a large reservoir likely of rhyolitic composition [*Singer et al.*, 2014].

Modeling the InSAR data indicates that the source geometry remains fairly constant in time, as found previously [*Feigl et al.*, 2014]. On the other hand, the rate of vertical displacement has evolved with time, as indicated by the good fit of the double exponential model to the InsAR data. Its mean squared error (MSE) of $\sigma_0^2 = 25$ is significantly better than that using the constant-rate model (Figure S4) where $\sigma_0^2 = 54$, as indicated by an F test with 95% confidence. A piecewise linear parameterization with six changes in rate reaches a better fit (Figure S5). We prefer the double exponential solution, because it is smooth in time and explains the post-2012 signal well. We cannot identify any precursory deformation or determine the exact epoch t_0 of the uplift episode because no useable interferometric pair exists between 2004 and 2007. On 27 February 2010, a large M_w 8.8 megathrust earthquake struck offshore central Chile, about 200 km west of Laguna del Maule [*Vigny et al.*, 2011]. The transition from increasing rates to decreasing rates, in March 2010, might be related to this regional stress change, as suggested for other volcanoes [*Pritchard et al.*, 2013]. The trends in InSAR and GPS agree for the time interval between 2012 and 2014 within their uncertainties (Figure S9).

Newman et al. [2001] have modeled the 1997–1998 uplift of the Long Valley caldera using a double exponential model like that described above, with $\tau_1 = 61$ days and $\tau_2 = 64$ days. These values are significantly shorter than at LdM, where $\tau_1 = 2.4$ years and $\tau_2 \geq 10$ years, although the second time constant is only weakly constrained. The exponential increase of the displacement rate could be explained by an intrusion of magma into the reservoir and/or the pressurization of fluids. The magnitude of such processes would control the timescale and thus the amount of displacement at the surface. The second time interval of exponentially decaying rates could be explained by viscoelastic relaxation of the crust; then the difference in time constants would be related to the rheological properties of the crust surrounding the reservoir [e.g., *Jellinek and DePaolo*, 2003].

Similarly, rapid rates of inflation have been observed at other volcanoes over shorter timescales (Figure 5a). For comparison, we have compiled and modeled available geodetic time series from examples of recent, well-studied deformation episodes including the following volcanic systems: Long Valley caldera [*Newman et al.*, 2001], Yellowstone, and Three Sisters [*Riddick and Schmidt*, 2011] (Figures 5, S7, and S8), using the same double exponential model. The estimated characteristic time constants vary between 0.2 and 10 years for uplift episodes lasting between 2 and 14 years (Figure 5a).

To emphasize the similarities, we consider the time series in terms of normalized displacement:

$$u'(t) = u(t)/(u_{\max} - u_0), \tag{3}$$

where $u_{\max}$ is the maximum vertical displacement, and u_0 is the displacement value at t_0, as a function of normalized time:

$$t' = (t - t_0)/(t_{\max} - t_0), \tag{4}$$

where t_0 is the onset epoch of uplift, and $t_{\max}$ is the time when the rate of vertical displacement becomes negligible, such that $t_0 \leq t_* \leq t_{\max}$. The epoch $t_{\max}$ is arbitrarily set to the last measurement epoch for LdM and Three Sisters, which are still showing uplift. The temporal evolution of the deformation follows the same pattern for each of these different volcanic systems. The normalized displacement u' as a function of the normalized time t' since the onset of inflation reveals a surprisingly similar pattern (Figure 5b), consistent with the hypothesis that similar processes are at work. For these volcanic systems, the displacement rate increases exponentially at the beginning of each deformation episode. The uplift rates then begin to slow (at t_*) and eventually pause and/or change to subsidence (at $t_{\max}$). The transitions from uplift to subsidence at both Yellowstone [*Chang et al.*, 2010] (Figure S7) and Long Valley [*Newman et al.*, 2001] were related to large seismic events and/or hydrothermal changes, but no eruption occurred. Indeed, these mechanisms could have relieved some of the stress accumulated during pressurization of the magma system, thus slowing the rate of deformation.

At LdM, although at least a dozen other episodes of seismicity have been reported by OVDAS from preliminary results, the only seismic swarm that appears to coincide with a significant change in the GPS estimates of vertical velocity is the largest one (in cumulative magnitude) on 11–12 January 2013.

5. Conclusions

Geodetic results indicate that an inflation episode began between 2004 and 2007 at LdM volcanic field in Chile and has continued through at least November 2014. The inflation pattern covers the entire postglacially erupted portion of the volcanic field. Based on the time series analysis of the InSAR data, we interpret the unrest in two time intervals after its onset. The uplift rate increased exponentially from zero to more than 400 mm/yr in early 2010, but began to decrease exponentially in March 2010 and eventually slowed to less than 220 mm/yr in 2014. The recent trend is confirmed by GPS measurements at the same location to be 192 ± 3 mm/yr from January 2013 to November 2014. The decrease in uplift rate in January 2013 coincides with the largest episode of high recorded seismicity (Figure 4). A comparison with episodes of unrest at three other volcanic systems reveals (1) the high rate of deformation (more than 200 mm/yr), (2) the long timescale (more than 8 years) of the unrest episode at LdM, and (3) a temporal evolution similar to inflation episodes at other volcanoes. We can expect the rate of uplift to keep decreasing before changing to subsidence or pausing prior to the next inflation event [e.g., *Tilling*, 2008].

Acknowledgments
We thank the RAMSAC CORS Network from Instituto Geografico Nacional de Argentina for access to their GPS data, which were used for part of this study. We thank Christophe Vigny and Jaime Campos of the International Associated Laboratory Montessus de Ballore (LIA-MB) for sharing GPS data from station MAUL. We appreciate the logistical assistance generously provided by Carlos Cardona and Fernando Gil at OVDAS, as well as Francisco Delgado, and Tor Stetson-Lee. We are especially grateful to "Don Luis" Torres for his gracious hospitality and nautical expertise. We also thank Nathan Andersen, Brad Singer, Elena Baluyut, Tabrez Ali, and the "LdM team" for helpful discussions. Detailed reviews from Michael Poland, Matthew Pritchard, and Francisco Delgado improved the manuscript. This research was partially supported by grants from NASA (NNX12AO37G), U.S. National Science Foundation (EAR-1411779), as well as support from the Weeks family and the G.P. Woollard fund. We acknowledge SAR data from the following space agencies: ASI (COSMO-Skymed), DLR (TSX), JAXA (ALOS), ESA (ERS and ENVISAT), and NASA (UAVSAR), as well as the coordination by the Supersites Initiative. The Generic Mapping Tool software was used to produce several maps [*Wessel and Smith*, 1998]. The authors thank Michael Poland, Francisco Delgado, and Matthew Pritchard for their assistance in critically and constructively evaluating this paper.

The Editor thanks Michael Poland, Franciso Delgado, and Matthew Pritchard for their assistance in evaluating this paper.

References

Ali, S., and K. Feigl (2012), A new strategy for estimating geophysical parameters from InSAR data: Application to the Krafla central volcano in Iceland, *Geochem. Geophys. Geosyst.*, *13*, Q06005, doi:10.1029/2012GC004112.

Beauducel, F., P. Briole, and J. -L. Froger (2000), Volcano-wide fringes in ERS synthetic aperture radar interferograms of Etna (1992–1998): Deformation or tropospheric effect?, *J. Geophys. Res.*, *105*(B7), 16,391–16,402, doi:10.1029/2000JB900095.

Berrino, G., G. Corrado, G. Luongo, and B. Toro (1984), Ground deformation and gravity changes accompanying the 1982 Pozzuoli uplift, *Bull. Volcanol.*, *47*(2), 187–200, doi:10.1007/BF01961548.

Bianchi, R., A. Coradini, C. Federico, G. Giberti, P. Lanciano, J. P. Pozzi, G. Sartoris, and R. Scandone (1987), Modeling of surface deformation in volcanic areas: The 1970–1972 and 1982–1984 crises of Campi Flegrei, Italy, *J. Geophys. Res.*, *92*(B13), 14,139–14,150, doi:10.1029/JB092iB13p14139.

Cayol, V., J. H. Dieterich, A. T. Okamura, and A. Miklius (2000), High magma storage rates before the 1983 eruption of Kilauea, Hawaii, *Science*, *288*(5475), 2343–2346, doi:10.1126/science.288.5475.2343.

Chang, W. -L., R. B. Smith, C. Wicks, J. M. Farrell, and C. M. Puskas (2007), Accelerated uplift and magmatic intrusion of the Yellowstone caldera, 2004 to 2006, *Science*, *318*(5852), 952–956, doi:10.1126/science.1146842.

Chang, W. -L., R. B. Smith, J. Farrell, and C. M. Puskas (2010), An extraordinary episode of Yellowstone caldera uplift, 2004–2010, from GPS and InSAR observations, *Geophys. Res. Lett.*, *37*, L23302, doi:10.1029/2010GL045451.

Davis, P. M. (1986), Surface deformation due to inflation of an arbitrarily oriented triaxial ellipsoidal cavity in an elastic half-space, with reference to Kilauea volcano, Hawaii, *J. Geophys. Res.*, *91*(B7), 7429–7438, doi:10.1029/JB091iB07p07429.

Del Gaudio, C., I. Aquino, G. Ricciardi, C. Ricco, and R. Scandone (2010), Unrest episodes at Campi Flegrei: A reconstruction of vertical ground movements during 1905–2009, *J. Volcanol. Geotherm. Res.*, *195*(1), 48–56, doi:10.1016/j.jvolgeores.2010.05.014.

Dieterich, J. H., and R. W. Decker (1975), Finite element modeling of surface deformation associated with volcanism, *J. Geophys. Res.*, *80*(29), 4094–4102, doi:10.1029/JB080i029p04094.

Dzurisin, D. (2007), *Volcano Deformation: New Geodetic Monitoring Techniques*, Springer, Berlin.

Feigl, K. L., and C. H. Thurber (2009), A method for modelling radar interferograms without phase unwrapping: Application to the M 5 Fawnskin, California earthquake of 1992 December 4, *Geophys. J. Int.*, *176*(2), 491–504, doi:10.1111/j.1365-246X.2008.03881.x.

Feigl, K. L., H. Le Mével, S. T. Ali, L. Córdova, N. L. Andersen, C. DeMets, and B. S. Singer (2014), Rapid uplift in Laguna del Maule volcanic field of the Andean Southern Volcanic zone (Chile) 2007–2012, *Geophys. J. Int.*, *196*(2), 885–901, doi:10.1093/gji/ggt438.

Fournier, T., M. Pritchard, and S. Riddick (2010), Duration, magnitude, and frequency of subaerial volcano deformation events: New results from Latin America using InSAR and a global synthesis, *Geochem. Geophys. Geosyst.*, *11*, Q01003, doi:10.1029/2009GC002558.

Grandin, R., et al. (2009), September 2005 Manda Hararo-Dabbahu rifting event, Afar (Ethiopia): constraints provided by geodetic data, *J. Geophys. Res.*, *114*, B08404, doi:10.1029/2008JB005843.

Henderson, S., and M. Pritchard (2013), Decadal volcanic deformation in the Central Andes Volcanic Zone revealed by InSAR time series, *Geochem. Geophys. Geosyst.*, *14*, 1358–1374, doi:10.1002/ggge.20074.

Hildreth, W., J. Fierstein, E. Godoy, R. E. Drake, and B. Singer (1999), The Puelche Volcanic Field: Extensive Pleistocene rhyolite lava flows in the Andes of central Chile, *Rev. Geol. Chile*, *26*, 275–309, doi:10.4067/S0716-02081999000200008.

Hildreth, W., E. Godoy, J. Fierstein, and B. Singer (2010), Laguna del Maule volcanic field: Eruptive history of a Quaternary basalt-to-rhyolite distributed volcanic field on the Andean range crest in central Chile, *Servicio Nacional de Geología y Minería–Chile Boletin*, *63*, 142.

Jellinek, A. M., and D. J. DePaolo (2003), A model for the origin of large silicic magma chambers: Precursors of caldera-forming eruptions, *Bull. Volcanol.*, *65*(5), 363–381, doi:10.1007/s00445-003-0277-y.

Lu, Z., D. Mann, J. T. Freymueller, and D. J. Meyer (2000), Synthetic aperture radar interferometry of Okmok volcano, Alaska: Radar observations, *J. Geophys. Res.*, *105*(B5), 10,791–10,806, doi:10.1029/2000JB900034.

Massonnet, D. (1997), Producing ground deformation maps automatically: The DIAPASON concept, in *Geoscience and Remote Sensing, 1997. IGARSS'97. Remote Sensing-A Scientific Vision for Sustainable Development., 1997 IEEE International*, vol. 3, edited by T. I. Stein, pp. 1338–1340, IEEE., Piscataway, N. J. doi:10.1109/IGARSS.1997.606441

Newman, A., T. H. Dixon, G. Ofoegbu, and J. Dixon (2001), Geodetic and seismic constraints on recent activity at Long Valley caldera, California: Evidence for viscoelastic rheology, *J. Volcanol. Geotherm. Res.*, *105*(3), 183–206, doi:10.1016/S0377-0273(00)00255-9.

Newman, A. V., et al. (2012), Recent geodetic unrest at Santorini caldera, Greece, *Geophys. Res. Lett.*, *39*, L06309, doi:10.1029/2012GL051286.

Okada, Y. (1985), Surface deformation due to shear and tensile faults in a half-space, *Bull. Seismol. Soc. Am.*, *75*(4), 1135–1154.

Orsi, G., L. Civetta, C. D. Gaudio, S. de Vita, M. D. Vito, R. Isaia, S. Petrazzuoli, G. Ricciardi, and C. Ricco (1999), Short-term ground deformations and seismicity in the resurgent Campi Flegrei caldera (Italy): An example of active block-resurgence in a densely populated area, *J. Volcanol. Geotherm. Res.*, *91*(2–4), 415–451, doi:10.1016/S0377-0273(99)00050-5.

Papoutsis, I., X. Papanikolaou, M. Floyd, K. Ji, C. Kontoes, D. Paradissis, and V. Zacharis (2013), Mapping inflation at Santorini volcano, Greece, using GPS and InSAR, *Geophys. Res. Lett.*, *40*, 267–272, doi:10.1029/2012GL054137.

Parks, M. M., et al. (2012), Evolution of Santorini volcano dominated by episodic and rapid fluxes of melt from depth, *Nat. Geosci.*, *5*(10), 749–754.

Pritchard, M., J. Jay, F. Aron, S. Henderson, and L. Lara (2013), Subsidence at southern Andes volcanoes induced by the 2010 Maule, Chile earthquake, *Nat. Geosci.*, *6*(8), 632–636, doi:10.1038/ngeo1855.

Pritchard, M. E., and M. Simons (2002), A satellite geodetic survey of large-scale deformation of volcanic centres in the central Andes, *Nature*, *418*(6894), 167–171, doi:10.1038/nature00872.

Riddick, S., and D. Schmidt (2011), Time-dependent changes in volcanic inflation rate near Three Sisters, Oregon, revealed by InSAR, *Geochem. Geophys. Geosyst.*, *12*, Q12005, doi:10.1029/2011GC003826.

Schmidt, D. A., and R. Bürgmann (2003), Time-dependent land uplift and subsidence in the Santa Clara valley, California, from a large interferometric synthetic aperture radar data set, *J. Geophys. Res.*, *108*(B9), 2416, doi:10.1029/2002JB002267.

Singer, B., et al. (2014), Dynamics of a large, restless, rhyolitic magma system at Laguna del Maule, southern Andes, Chile, *Geol. Soc. Am.*, *24*(12), 4–10, doi:10.1130/GSATG216A.1.

Sparks, R. (2003), Forecasting volcanic eruptions, *Earth Planet. Sci. Lett.*, *210*(1–2), 1–15, doi:10.1016/S0012-821X(03)00124-9.

Tilling, R. I. (2008), The critical role of volcano monitoring in risk reduction, *Adv. Geosci.*, *14*, 3–11, doi:10.5194/adgeo-14-3-2008.

Trasatti, E., M. Bonafede, C. Ferrari, C. Giunchi, and G. Berrino (2011), On deformation sources in volcanic areas: Modeling the Campi Flegrei (Italy) 1982–84 unrest, *Earth Planet. Sci. Lett.*, *306*(3), 175–185, doi:10.1016/j.epsl.2011.03.033.

Vigny, C., et al. (2011), The 2010 M_W 8.8 Maule megathrust earthquake of Central Chile, monitored by GPS, *Science*, *332*(6036), 1417–1421, doi:10.1126/science.1204132.

Wackerly, D., W. Mendenhall, and R. Scheaffer (2007), *Mathematical Statistics With Applications*, Cengage Learning, Belmont, Calif.

Walter, T. R., and M. Motagh (2014), Deflation and inflation of a large magma body beneath Uturuncu volcano, Bolivia? Insights from InSAR data, surface lineaments and stress modelling, *Geophys. J. Int.*, *198*(1), 462–473, doi:10.1093/gji/ggu080.

Wessel, P., and W. H. Smith (1998), New, improved version of generic mapping tools released, *Eos Trans. AGU*, *79*(47), 579–579, doi:10.1029/98EO00426.

Wright, T. J., et al. (2012), Geophysical constraints on the dynamics of spreading centres from rifting episodes on land, *Nat. Geosci.*, *5*(4), 242–250, doi:10.1038/ngeo1428.